Journal of Catalysis 242 (2006) 340-348

Carbon incorporation during ethene oxidation on Pd(111) studied by in-situ X-ray photoelectron spectroscopy at $2x10^{-3}$ mbar

H. Gabasch [a,d], E. Kleimenov [a], D. Teschner [a], S. Zafeiratos [a], M. Hävecker [a], A. Knop-Gericke [a], R. Schlögl [a],D. Zemlyanov [b,c], B. Aszalos-Kiss [b], K. Hayek [d], B. Klötzer [d*]

[a]Anorganische Chemie, Fritz-Haber-Institut der Max-Planck-Gesellschaft, Faradayweg 4–6, 14195 Berlin, Germany
[b]Materials and Surface Science Institute and Physics Department, University of Limerick, Limerick, Ireland
[c]Purdue University, Birck Nanotechnology Center, 1205 West State Street, West Lafayette, IN 47907-2057, USA
[d]Institut für Physikalische Chemie, Universität Innsbruck, Innrain 52A, A-6020 Innsbruck, Austria

[*] Corresponding author: e-mail bernhard.kloetzer@uibk.ac.at, Tel.: +43 512 507 5071, Fax: +43 512 507 2925

Received 3 May 2006; revised 21 June 2006; accepted 25 June 2006. Available online 4 August 2006.

Abstract

The oxidation of ethene on the Pd(111) surface was studied in the temperature range 330 K to 923 K by in-situ XPS and mass spectrometry both during heating and cooling in a reaction mixture of $5x10^{-4}$ mbar C_2H_4 and $1.5x10^{-3}$ mbar O_2. Carbon-containing surface species were found to be strongly predominant over oxygen species within the whole temperature range, despite the excess of oxygen in the gas phase. Diffusion of carbon into the palladium bulk started at 480 K, leading at ~500 K to the appearance of an electronically altered, dissolved carbon phase with a C1s binding energy of 284.45eV, which extended over several layers in the near-surface region and was stable up to ~650 K. This spectroscopic trend was clearly related to a pronounced shift of catalytic selectivity toward CO. Above 660K the dissolved carbon species decomposed and the reaction took place on an adsorbate-depleted Pd metal surface, with CO as the main product. During the cooling ramp the same surface-near carbon modification formed at a 70 degree lower threshold temperature, inducing a pronounced hysteresis of the catalytic selectivity.

Keywords: Palladium, Pd(111), Ethene oxidation, High pressure in situ XPS, Subsurface carbon, Dissolved carbon, Temperature programmed reaction, Kinetic hysteresis

1. Introduction

It is known that the catalytic properties of palladium strongly depend on its oxidation state. On the one hand dispersed palladium metal is an important catalyst for hydrocarbon (in particular methane) combustion [1,2]. In case of methane oxidation e.g. on alumina-supported Pd, the catalytic activity of Pd is associated with the kinetic hysteresis between formation and decay of the highly active PdO phase [3,4].

On the other hand, palladium-containing supported catalysts are also frequently used in the selective oxidation of hydrocarbons, e.g. of ethene to acetaldehyde or to acetic acid [5-7], and of ethene plus acetic acid to vinyl acetate [8-11]. For these processes the catalytic importance of carbon residing in the subsurface region of a highly reduced state of the catalysts has already been recognized [5,10,12]. In case of unsupported Pd several modifications of the surface and the surface-near region are reported in literature, among them the formation of a well ordered hydride strongly promoting e.g. ethene hydrogenation [13], and a solid solution of carbon formed near the Pd surface by different carbon containing gases[14-16].

The main problem of previous ex-situ studies is of course the stability of intermediate reactive species, since most of them are metastable and may only exist under certain reaction conditions. As predicted by theoretical calculations of oxygen subsurface migration [17,18], a certain chemical potential of gas phase oxygen is needed to establish a supersaturation of adsorbed oxygen on the surface, sufficient to stabilize the “dissolved” oxygen atoms beyond the first atomic layer, which are energetically less favourable than surface-adsorbed O-atoms. For carbon the situa-

tion appears to be different. As has been revealed experimentally in our previous work and also has been substantiated by DFT calculations [18,19], the adsorbed carbon atoms need to overcome an activation barrier of 107 kJ/mol to pass the surface Pd layer (59-78 kJ/mol according to recent theory work[18]), but then become energetically stabilized in the subsurface or bulk dissolved state [18,20,21]. The activation barrier for C migration inside the bulk is considerably lower, at 65 kJ/mol [20] The amount of carbon expected within the first atomic layers will therefore depend strongly on temperature, pressure and time. In our previous UHV work it was possible to quantify the irreversible rate of carbon uptake resulting from ethane dissociation through the surface Pd layer [19], but all measurements under UHV conditions are basically hampered by unknown distribution of carbon among surface-near and deeper bulk regions. It is therefore necessary to investigate the Pd catalyst in situ, in order to detect species on and also below the surface which are *only* stable under steady reaction conditions. X-ray photoelectron spectroscopy (XPS) using tunable synchrotron light is one of the most powerful *in-situ* techniques because it can monitor both the surface and the surface-near regions with high sensitivity, including the possibility of information depth variation.

2. Experimental

Conventionally, XPS is operated under UHV, since the photoelectrons are strongly scattered in a high-pressure gas phase. To overcome these limitations, high-pressure XPS chambers were designed in the late 1970's [22]. A number of high-pressure XPS experiments have been performed since then [23-25]. The in situ XPS setup used for this study employs differentially pumped electrostatic lenses, and allows to measure the sample in a gaseous environment (batch flow reactor mode) at pressures of up to 1 mbar.

The experiments were performed at beamline U49/2-PGM1 at BESSY in Berlin. The high-pressure XPS setup is described elsewhere [26]. The photoelectron binding energy (BE) was calibrated with respect to the Fermi edge. The sample, a (111)-oriented Pd single crystal, was mounted on a temperature-controlled heating stage. The temperature was measured by a chromel-alumel thermocouple spot-welded onto the side of the sample. The sample was heated by an IR laser from the rear. The sample cleaning procedures consisted of repeating cycles of Ar^+ sputtering at room and elevated temperature, annealing up to 950 K in UHV, and exposure to O_2 followed by flashing at 950 K for 60 seconds in UHV. The sample cleanness was checked by XPS. The Pd(111) single crystal sample was positioned inside a high-pressure cell 2 mm away from a 1 mm aperture, the entrance to a differentially pumped electrostatic lens and to the hemispherical analyser.

In order to study activity, selectivity and chemical state of the catalyst during ethene oxidation, a reaction mixture of ethene and oxygen (ratio 1:3) was allowed to flow through its reaction chamber. The total flow rate was empirically adjusted for a sufficiently sensitive detection of the reaction products by a QMS, which was supplied with a minor portion of the reaction mixture via a defined capillary leak. In our experimental setup neither the exact supply rate of the reactants through the leak valves nor the effective pump rate of the reaction chamber could be calibrated with reasonable precision. Thus we have to limit ourselves to the partial pressure data of reactants and products in the reaction chamber under steady reaction conditions, and we can not quantify turnover rates. The partial pressure data were calculated on the basis of the decrease of the QMS intensities of oxygen (m/z = 32) and ethene (m/z = 27) and of the increase of CO (m/z = 28), water (m/z = 18) and CO_2 (m/z = 44) induced by the catalytic reaction. The total reactant pressure and the actual partial pressure ratio of ethene and oxygen were measured by an ionization gauge prior to the onset of the reaction (cold catalyst), thereby accounting for their relative ionization probability. On this basis the m/z = 27 ethene and m/z = 32 oxygen QMS signals could be calibrated. Since in our experiment no measurable amounts of molecular reaction products (acetic acid, acetaldehyde...) were detectable, the reaction stoichiometry is limited to the irreversible formation of water, CO and CO_2:

$$C_2H_4 + (3\text{-}x)O_2 \rightarrow (2x)CO + (2\text{-}2x)CO_2 + 2\ H_2O$$
$$\text{with} \quad (0 < x < 1)$$

The known relative detection sensitivity of CO and CO_2 in the QMS was used to determine x

from the m/z=28 and m/z=44 signals. Since the mass 28 signal represents a superposition of the ethene and CO molecule ion contributions, at first the appropriate intensity contribution of the ethene-induced m/z=28 signal was subtracted from the total m/z=28 signal, in order to extract the CO-related contribution. This was done by amplifying the solely ethene-related m/z=27 signal curve, which is not influenced by CO, by the known (separately determined) signal ratio of m/z=28 to m/z=27 for clean ethene, followed by subtraction.

In order to back-check the described quantification of the individual partial pressures, the sum of the CO and CO_2 partial pressures was compared with the ethene partial pressure change and a very good agreement was verified using a factor of 2. Finally, the sum of all product partial pressures (CO, CO_2 and water) equalled the reaction-induced ethene pressure change multiplied by a factor of 4, in accordance with the stoichiometry given above.

The temperature-programmed catalysis experiments involved heating with a linear ramp rate of 10 K/min from 330 K to 923 K, holding the temperature at 923 K for 3 min, and cooling, again with a linear ramp of 10 K/min, to 423 K. During this temperature program both the composition of the gas phase was continuously measured with the QMS and XPS spectra (O1s, C1s, Pd3d region, fermi edge and survey spectra in order to check for contaminants, photon energy 650 eV) were continuously recorded. The deconvolution of the $Pd3d_{5/2}$ XP spectra involved an

asymmetric Gausso-Lorentzian sum function in analogy to [27,28]. Accordingly, the clean Pd(111) Pd3d$_{5/2}$ peak was deconvoluted into two components, an asymmetric bulk and a symmetric surface component according to [29]. The spectra generated by this procedure were optimised by least-squares fits to the experimental data with a Shirley-type background considered. The derived binding energies (334.93eV for the bulk and 334.63 for the surface component), which are in very good agreement with previous peak fits [29,30] and their shape parameters (FWHM, asymmetry and mixing factor of Gausso-Lorentzian sum) were kept within the constrains given in Table 1. In order to determine the adsorbate and carbon induced components in the Pd3d$_{5/2}$ spectra only the binding energies and the peak area were optimised by the fitting procedure. The FWHM and mixing ratio were again kept within the same constraints as the bulk and surface components. Table 1 summarizes the particular components and their fitting parameters.

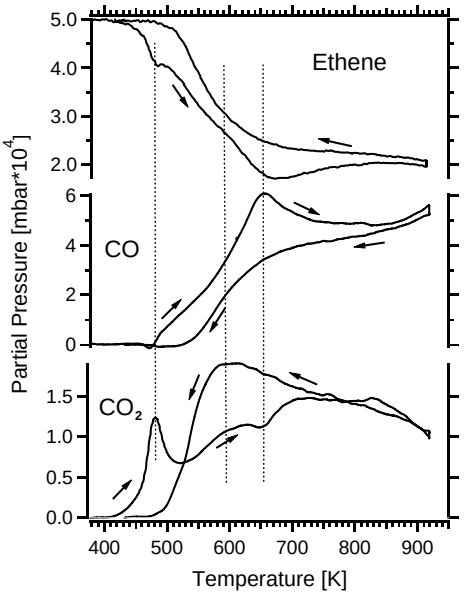

Figure 1: Partial pressures of CO_2, CO and ethene during the oxidation of ethene plotted against temperature

3. Results

3.1. Heating cycle

Fig. 1 shows the partial pressures of ethene and of the carbon oxide products plotted vs. temperature. The traces of CO and CO_2 both show a strong hysteresis behaviour. Water formation is omitted in Fig.1 since its partial pressure change closely corresponded to the inverse ethene pressure change multiplied by 2. The top graph shows the partial pressure of ethene and reflects total conversion. The reaction starts at > 430 K, a temperature which is close to results from previous studies on complete thermal ethene decomposition [19]. It was shown that ethene starts to decompose to carbon and hydrogen in the temperature range above 410 K and that C subsurface migration starts at T>440 K both on the Pd(111) surface [19] and the Pd(110) surface [31]. The initial activity increase exhibits already a remarkable "fine structure", as a minimum in the ethene partial pressure evolves at 480 K (left dotted line in Fig.1) and the selectivity for CO_2 formation is almost 100% (compare also the respective selectivity plot in Fig.8), i.e. CO formation has not yet started. In a small window between 480 and 500 K the ethene conversion stagnates and the CO_2 formation slows down, reaching a first minimum at 520 K, and exactly in this range CO starts to be formed with increasing rate. The catalyst now becomes highly active with respect to CO formation and both ethene conversion and CO partial pressure reach a peak at 660 K (p_{CO} = 6*10^{-4} mbar), in contrast to CO_2 formation, which shows only a shallow increase up to about 620 K and exhibits a minimum at 660 K (Fig.1, right dotted line). In general, the low temperature region (380 K to 660 K) is characterised by a strong activity increase from zero to the maximum value and a dramatic decrease of the CO_2 selectivity (given in Fig.8, derived from the data of Fig.1) from >90% to ~20%, and vice versa by a strong increase of the CO selectivity from <10% to ~80%.

From 660 K up to 923 K the activity with respect to ethene conversion remains in a relatively narrow range and the selectivity changes (CO vs. CO_2) are much less pronounced. CO remains the main product at high temperatures (Fig. 8). The CO_2 formation rate (Fig.1) and selectivity (Fig.8) increase from 660 to 750 K and then again decrease up to 923 K, as complemented by the inverse trend in CO formation and selectivity, the latter ranging in between 84% and 70% (CO_2 between 15% and 30 %).

The same description holds for the cooling cycle in between 923 K and 700 K: the selectivity pattern and the total activity are close to the values observed during heating, i.e. there are no strong hysteresis effects observed in this temperature range. The situation changes drastically below 700 K: CO formation is diminished quickly, but now *without* passing through a maximum at 660K, and approaches zero rate already at 520 K. In contrast, the CO_2 rate increases continuously between 923 K and 600 K, reaches a pronounced maximum at 600 K (Fig.1, middle dotted line) and then decreases steeply to approach zero rate at around 500 K. The low temperature maximum of CO_2 formation observed during heating at 480 K is missing. The data of Fig.1/ Fig.8 clearly show a pronounced hysteresis of the CO- and CO_2 formation rates and selectivities, giving rise to a *selectivity* hysteresis rather than a hysteresis in total activity.

In situ XPS spectra were recorded continuously during the temperature programmed reaction experiment, which are presented in the following figures. Fig.2 displays the C1s spectral region during the heating cycle. As indicated by the low temperature spectra (330 K - 461 K), the Pd (111) surface is covered by carbon containing surface

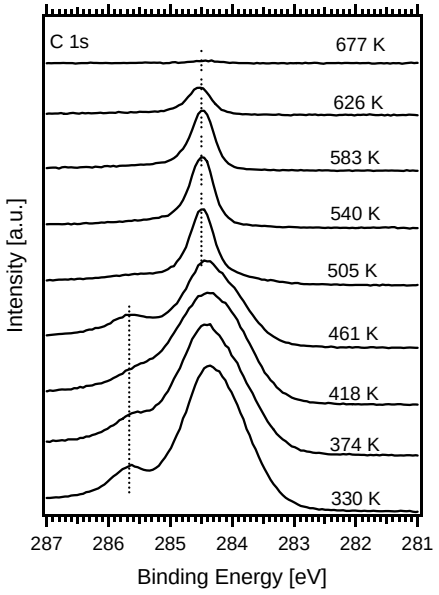

Figure 2: C1s region recorded during heating from 330 K to 677 K. Photon Energy 650eV

species. The C1s signal shows a broad peak between 283 eV and 286 eV lacking of analyzable structural features. Already an adlayer consisting *only* of ethylidyne (e.g. from ethene adsorbed at 300 K) gives rise to a rather complex spectrum of 4 components in the range between 283.5 eV and 285 eV [32]. Moreover ethylidyne should gradually decompose above 350 K towards more dehydrogenated molecular adsorbates, e.g. ethinyl (CCH), and finally toward atomic carbon [19,33]. Therefore, and also because oxygenated intermediates may be additionally formed, we regard any meaningful deconvolution and assignment of peak components to known carbonaceous species as impossible on the basis of the present XPS data. Only a separate peak with a maximum at 285.65 eV is most likely due to adsorbed CO, corresponding to a C1s signal usually observed at binding energies between 285.53 eV for low CO coverage and 285.80 eV for saturation coverage [34]. There are no hints of more strongly oxygenated carbon species such as formate or acetate on the surface causing high BE features above 286 eV [35]. From 461 K to 505 K the C1s spectrum is completely changed. The broad C1s intensity between 283 eV and 285.5 eV disappears, and as well the intensity at 285.65 eV characteristic of adsorbed CO. Instead a sharp, symmetric single C1s peak (FWHM of 0.4 eV, spectral resolution ~ 0.1. eV) is observed at 284.50 eV, indicating the presence of a single C species. The BE shift relative to adsorbed CO is in good agreement with theoretical results calculated for dissolved carbon atoms [18]. This peak exhibits an approximately constant intensity up to 583 K and vanishes above 677 K.

In analogy to the effects observed for the C1s region in Fig.2, the Pd3d$_{5/2}$ peaks displayed in Fig. 3a show an additional shoulder at the high BE side in between 358 K and 444 K, characteristic of an adsorbate covered Pd(111) metal surface [34]. The dotted line indicates the peak position of the Pd bulk component according to [29]. The presence and constant intensity of the bulk Pd component proves that in this temperature range the gas - surface interaction is indeed limited to the surface, as will be shown by the peak deconvolution of Fig. 3b.

A strong change is observed as the temperature becomes higher and CO formation starts (480 K in Fig.1). The peak maximum shifts from the original bulk Pd position at 334.9 eV up to 335.4 eV and the peak becomes nearly symmetric. A very similar spectrum persists up to 568 K. At 611 K the bulk Pd component contributes again more strongly to the spectrum, and above 654 K the whole spectrum becomes rather characteristic of clean Pd metal (peak maximum again at 334.9 eV) [29]. The assignment of this spectrum to cleaned-off Pd metal is corroborated by the absence of measurable C1s and O1s intensity at this temperature (for C1s see Figs. 2 and 5). The Pd3p/O1s region was monitored throughout the whole TPR experiment, but this spectra series is not shown since it exhibited no detectable O1s intensity contribution. Both O(ad) or surface-oxide related O contributions could be expected and, if present, should be superimposed as a low BE shoulder in the Pd3p-O1s spectral range (BE 528.9 to 530.4 eV) [36]. Our detection limit for such species was deduced from a previous study of Pd(111) oxidation [36] in the same experimental setup under otherwise very similar conditions, and is below 0.05 ML. We therefore conclude that the steady concentration of atomic oxygen species remains below the detection limit over the *whole* temperature range. Also the detection of small amounts of carbon oxygenates, in particular of CO (see CO induced component in the C1s spectra of Figs.2 and 5 between 330 K and 500 K) in the O1s spectra is hampered by the strong overlap with the broad Pd3p emission with a maximum at BE = 532 eV. Above 650 K the surface therefore can be considered as largely carbon- and oxygen depleted and the spectrum of almost clean Pd(111) is observed.

Selected Pd3d$_{5/2}$ profiles of Fig. 3a were subjected to a standard peak deconvolution using an asymmetric Gausso-Lorentzian sum function applied after Shirley-type background correction, and are shown in Fig. 3b. Table 1 provides a summary of the BE of the assignable Pd3d spectral components, on which the deconvolution was based. The experimental data (circles) are reproduced by the sum of three main components, which are assigned to the clean Pd metal surface layer at 334.63 eV, the Pd metal bulk at 334.93 eV and the Pd component of the electronically altered Pd_xC_y state at 335.34 eV. Only in the 358 K spectrum an adsorbate-induced component at 335.52 eV was added to the deconvolution, in agreement with the presence of hydrocarbon adsorbates and CO (at 285.6 eV in Figs. 2 and 5) at T<500 K. Due to the adsorbate-induced shift of surface Pd the clean Pd(111) surface component at 334.63 eV is missing at 358 K.

At 568 K, during heating, the bulk Pd component has already decreased and the Pd_xC_y component has strongly gained in intensity. This trend is reverted again above 611 K and at 846 K the presence of a mostly adsorbate-depleted

Table 1: Spectral components and parameters of fitting to the $Pd3d_{5/2}$ photoemission peak.

XPS peak	Assignment	Pd 3d5/2 peak		
		BE [eV]	FWHM [eV]	% Lorentzian
Pd (111)	Bulk	334.93 ±0.02	0.75±0.05	25±3 %
	Surface	334.63 ±0.04	0.75±0.05	25±3 %
Adsorbate induced		335.52 ±0.04	0.75±0.05	25±3 %
Dissolved carbon induced	Pd_xC_y	335.34 ±0.03	0.75±0.05	25±3 %

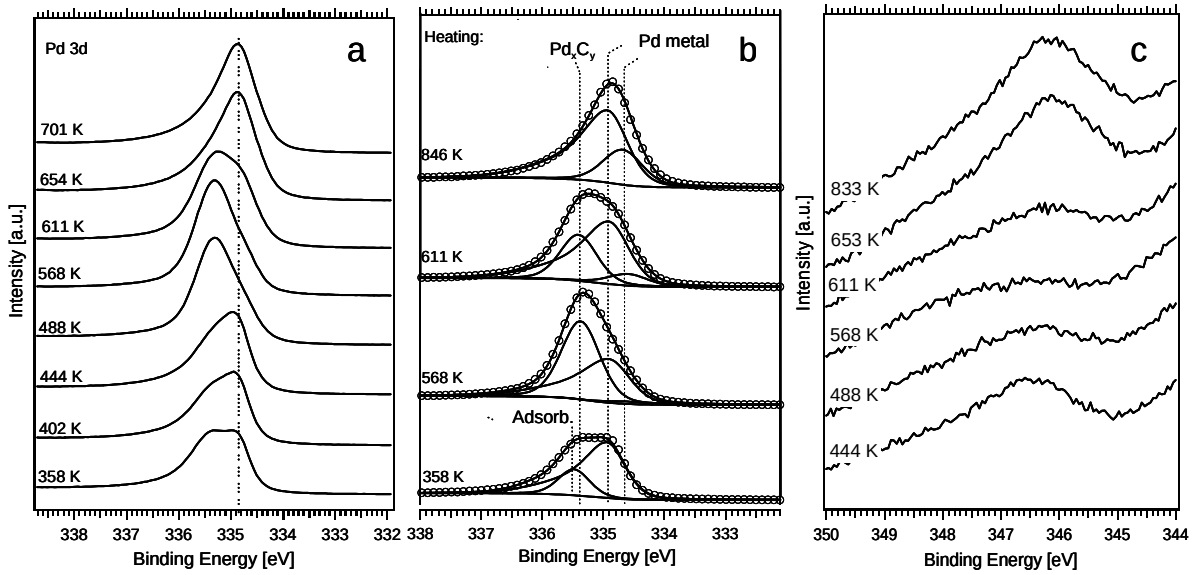

Figure 3: (a) $Pd3d_{5/2}$ region recorded during heating from 358 K to 701 K. (b) Selected $Pd3d_{5/2}$ photoemission spectra deconvoluted according to Table 1. (c) Palladium plasmon excitation monitored during heating. Photon Energy for all spectra 650 eV.

metallic catalyst is indicated by the adequate contribution of the clean surface and bulk Pd metal components [29].

The strong suppression of the Pd metal bulk component at BE = 334.93 eV in the temperature region from 480 to 660 K indicates major alterations of the electronic state of the Pd(111) surface near region. In this respect, additional information could be derived from a detailed analysis of the characteristic Pd plasmon loss, which shifts a part of the $Pd3d_{3/2}$ photoelectrons toward higher BE by about 6.5 eV. The corresponding plasmon peak is shown in Fig. 3c, and exhibits a maximum intensity at approximately 346.4 eV (Pd $3d_{3/2}$ peak at 340.13 eV). Plasmon shifts of 6 to 7 eV were reported by Rocca et al. [37,38] and Netzer et al. [39] using angle resolved EELS. At low temperatures (444 K in Fig. 3c) the still metallic sample is only adsorbate-covered, and the plasmon peak is clearly visible. The intensity of the loss peak at 444 K in Fig. 3c is slightly smaller as compared to the adsorbate-depleted metal at T> 653 K, most likely due to the adsorbate layer present. This is in agreement with [39], wherein it was shown that e.g. a CO adlayer induces a lowering of the loss intensity. The spectra recorded between 488K and 611 K show that the plasmon vanishes, supporting major changes of the valence band structure of the Pd bulk within the XPS information depth. Above 653 K the plasmon peak reappears at an intensity ascribed to an adsorbate-depleted metal surface.

Additional support for major electronic changes between 480 K and 660 K comes from the observation of a pronounced shift of the highest occupied electronic states toward higher BE with respect to the metal Fermi level by

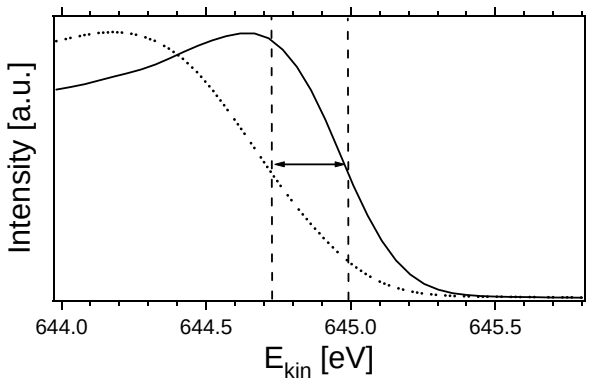

Figure 4: Fermi edge recorded during heating at 520 K (dotted line) and 680 K (solid line).

0.24 eV at 520 K, as demonstrated by Fig. 4. A simply surface-adsorbate covered Pd metal sample would not exhibit such behaviour, since the main fraction of photoelectrons originates from the layers below the terminal metal surface layer. The inelastic mean free path of 650 eV electrons is approx. 13 Å, and the fraction of photoelectrons from the first 5 Å is estimated to contribute less than 40 % [40]. We therefore conclude that the changes on the catalyst affect not only the top metal layer, but extend at least over the surface-near region observed by XPS. The perfect reversibility of the observed shift upon decay of the carbon-rich surface modification at >660 K proves that this effect exclusively affects the sample surface near region.

3.2. Cooling cycle

As shown in Fig 5, during cooling from 923 K down to 646 K the C1s intensitiy remains close to zero, as well as the O1s intensity (which is beyond the detection limit at any temperature), thus supporting the presence of a strongly adsorbate-depleted surface. Small amounts of C accumulate already at 646 K and below, as indicated by a single small peak at 284.50 eV. This peak quickly gains intensity as the temperature becomes lower than 603 K. At 506 K and below, the spectra develop a shoulder at the low binding energy side, which likely stems from carbonaceous species in a low oxidation state. Speculatively, ethylidyne (intensity maximum at 284.0 eV) [32] and more strongly dehydrogenated ethene fragments such as ethinyl (CCH) could be named [33]. A second peak at 285.65 eV (left dotted line in Fig. 5) appearing at T < 557 K is again attributed to CO, in analogy to Fig. 2. The main intensity contribution to the whole spectrum remains that of the dissolved C component at 284.50 eV over the whole temperature range down to 435 K. This result is in contrast to the 330 K – 461 K *heating* spectra shown in Fig.2. During heating the 284.50 eV component characteristic of dissolved C atoms should start to contribute to the C1s intensity above 480 K, as deduced from the increase of the related Pd_xC_y Pd3d component in Fig. 3a at 488 K.

Complementing the C1s data of Fig. 5, Fig. 6a displays the Pd3d$_{5/2}$ spectral range monitored during cooling.

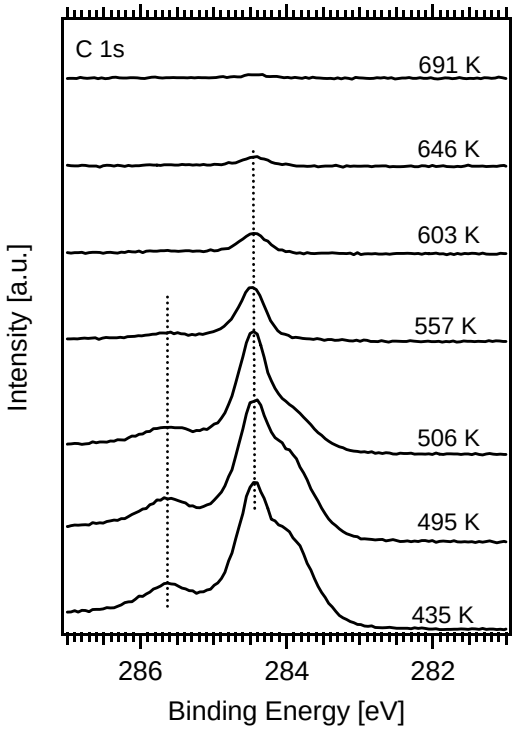

Figure 5:C1s region recorded during cooling from 691 K to 435 K. Photon Energy 650eV.

In Fig. 5, the first traces of carbon are visible at 646 K, but the amount of carbon increases to a substantial value at around 557 K. According to this increase in the Pd3d region also a pronounced change of the Pd3d peak shape is observed at T < 574 K. In analogy to the heating spectra (Fig. 3a between 488 K and 611 K) an increased contribution of a component at higher BE and vice versa the decrease of the Pd metal bulk component contribute to the change of peak shape. In contrast to the heating cycle these changes persist down to the lowest temperature (423 K), and the surface does not return into the adsorbate-covered metallic state observed in the beginning of the heating cycle (Fig. 3, T < 444 K). This difference is quantified in the selected deconvoluted spectra of the cooling cycle shown in Fig. 6b. At 529 K the Pd_xC_y component (335.34 eV) is strongly predominant and – although slightly reduced - remains predominant down to the lowest temperature.

On the basis of Fig 6a and b it is likely that the electronically altered state of the carbon doped catalyst observed during heating above 480 K (Fig. 3) becomes quenched during the cooling cycle and remains stable down to 400 K. This state is also characterised by the C1s contribution at 284.50 eV, which steadily grows during cooling down to 400 K (Fig. 5).

A more direct proof for the formation of the Pd_xC_y state during cooling below 611 K and its persistence below 480 K can be derived from the changes of the plasmon peak at 346.4 eV shown in Fig. 6c. Whereas the 574 K trace is still characteristic of the metallic state of the catalyst, at 529 K already a complete extinction of the plasmon excitation is observed. In contrast to the heating cycle (Fig.

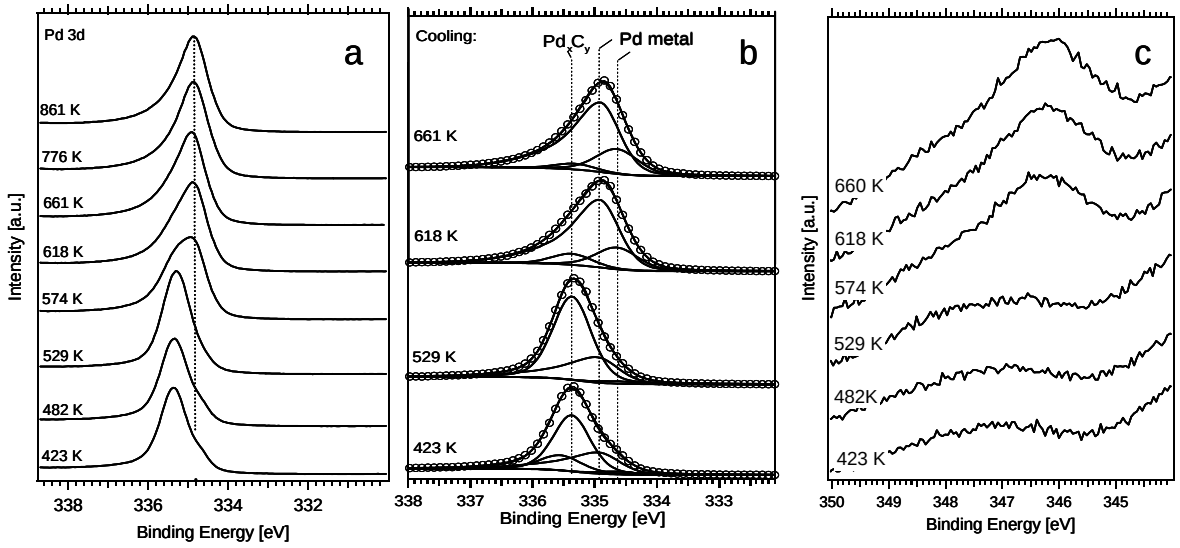

Figure 6: (a) Pd3d$_{5/2}$ region recorded during cooling from 861 K to 423 K. (b) Selected Pd3d$_{5/2}$ photoemission spectra deconvoluted according to Table 1. (c) Palladium plasmon excitation monitored during cooling. Photon Energy for all spectra 650eV.

3c, 444 K), the plasmon peak cannot be observed at the lowest temperature (Fig. 6c, 423 K), i.e. the catalyst *remains* in the Pd_xC_y state during cooling.

In order to prove the extended bulk nature of the Pd_xC_y species, depth profiling by variation of the incident photon energy was performed at a constant temperature of 488 K (Fig.7). Since the mean free path of an electron in a solid depends on its kinetic energy (KE), the escape depth of the photoelectrons varies with the incident photon energy ($h\nu$), according to KE = $h\nu$ - BE - Φ (where Φ is the work function). We recorded spectra at four different incident photon energies: 460, 590, 720, and 910 eV. These correspond to inelastic mean free path lengths of 5, 7, 9, and 12 Å, respectively (assuming that palladium remains the largely predominant constituent in the near-surface region) [40]. From Fig. 7 it is obvious that the relative contribution of the bulk Pd metal and the Pd_xC_y components changes only little with the information depth. The incorporated carbon affects not only the first layer of Pd(111) but extends at least over 12 Å, and we also may deduce that the concentration of carbon in Pd_xC_y decreases slightly within deeper layers, as suggested by the slight decrease of the Pd_xC_y to Pd bulk ratio with increasing IMFP. This result is important in view of a recent XRD study [41], analyzing the chemical state of alumina-supported palladium catalysts (1 and 3% Pd) during the oxidation of unsaturated hydrocarbons under O_2 sub-stoichiometric conditions. In [41] the formation of a new crystallographic phase with a larger lattice constant than that of clean Pd metal was reported, which was denoted "PdX" with X = oxygen. Lacking information about the chemical composition of this phase, the phase change was attributed to the formation of a Pd-oxygen compound, but on the basis of our work we rather suggest Pd modified by a considerable carbon loading.

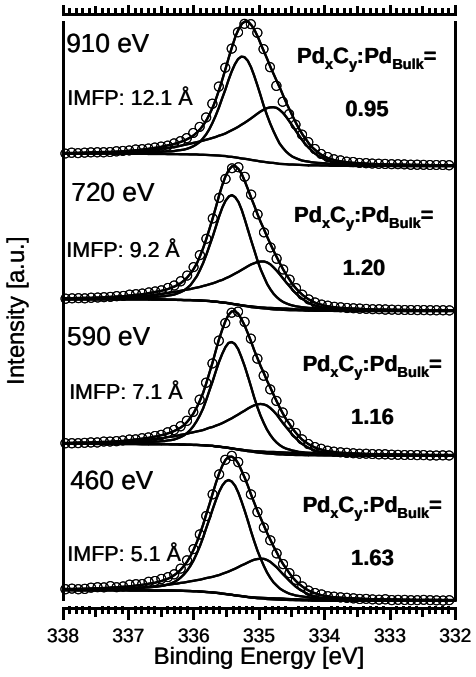

Figure 7: Pd3d$_{5/2}$ photoemission spectra recorded at 473 K and at the indicated photon energies. The information depth of the emitted electrons (inelastic mean free path) was calculated according to [40].

4. Discussion

In Fig. 8 the possible origin of the observed selectivity hysteresis is sketched on the basis of the intensity changes of the Pd3d Pd_xC_y component at 335.34 eV, representing the electronically altered state of the catalyst induced by the high subsurface/ dissolved carbon loading. The selectivities given in the lower graph of Fig. 8 are based on the fraction of the partial pressures with respect to the carbon oxide total pressure $p(CO)/(p(CO)+p(CO_2))*100\%$ and $p(CO_2)/(p(CO)+p(CO_2))*100\%$. This plot had to be limited to the temperature range where the overall reaction rate (ethene consumption) is already high enough. If – at the lowest temperatures - the partial pressures of CO and CO_2 are very low, i.e. close to the baseline, the relative error and the noise are too high to extract any useful value for the selectivity.

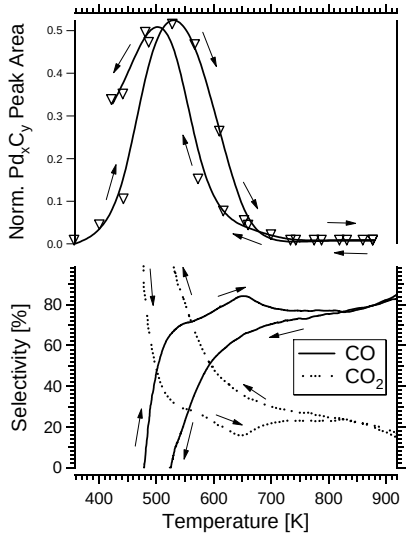

Figure 8: Top graph: temperature hysteresis of the dissolved carbon Pd_xC_y (335.34 eV) component.
Bottom graph: temperature hysteresis of the fractional contribution (in %) of p(CO) (solid line) and $p(CO_2)$ (dashed line) to the total pressure of the carbon oxide reaction products $p(CO) + p(CO_2)$.

4.1. Heating cycle

For clarity 3 distinct temperature regions are discussed.

A) Low temperature region up to 480 K: A Pd(111) metal surface covered by an adsorbate layer containing CO is present, the Pd3d Pd_xC_y intensity remains low (in [19] we have shown that ethene decomposition toward carbon becomes fast at T > 410 K and migration of carbon into the bulk at >480 K) and the main reaction product is CO_2. Between 461 K and 505 K the CO C1s signal at 285.4 eV (Fig. 2) vanishes, probably due to the increasing rate of the CO – oxygen reaction reflected by the increase of the CO_2 production (maximum at 480 K, Fig.1). At ~480 K the CO desorption rate from metallic Pd(111) is still relatively low [42,43] and the lifetime of the chemisorbed CO is probably high enough to get oxidized to CO_2 prior to desorption, according to a Langmuir- Hinshelwood reaction mechanism on the metal between O(ads) and CO(ads).

B) 480 K to 660 K: According to [19] in this temperature region the subsurface migration of surface-adsorbed carbon accelerates steeply. The Pd3d Pd_xC_y intensity passes through a pronounced maximum at 520 K. On the dissolved carbon phase CO becomes the main reaction product, which is formed at a steeply increasing rate, meaning that the oxidation mechanism on Pd_xC_y strongly boosts CO (from <10 % to >80%) and supresses CO_2 formation (from >90% to <20%, Fig. 8). For a tentative explanation we may think about a too short lifetime of CO on the Pd_xC_y phase to become oxidized by adjacent O atoms, which may also become quickly consumed by this extremely carbon-rich catalyst environment. This may lead to a suppression of the secondary CO oxidation toward CO_2. Generally spoken, it is very likely that CO_2 formation from C and O proceeds via intermediate CO, rather than through a single 3-body microkinetic process.

Recent work on CO adsorption on carbon-modified Rh(100) by Nieskens et al. [44] has revealed that both surface and subsurface carbon greatly influence CO adsorption. C(sub) shifts the average desorption temperature of CO to lower values, which would eventually result in a reduced CO equilibrium coverage (and microscopically in a reduced average CO lifetime) at e.g. 500 K.

C) 660 to 923 K: Beyond the decomposition limit of the dissolved carbon phase the Pd $3d_{5/2}$ spectrum becomes characteristic of an adsorbate-depleted Pd(111) metal surface. This transition is accompanied by a partial reversal of selectivity toward CO_2 up to 750 K (from <20% to ~25%). Above 750 K again a trend toward more CO (finally 85% CO vs. 15% CO_2 at 923 K) is obvious. As was concluded from the C1s and O1s spectra, in this temperature region both the C(ads) and O(ads) concentrations are below the detection limit, so it was not possible to trace the origin of these trends spectroscopically. A simplified but rather general concept could be again based on the lifetime ratio of adsorbed CO and oxygen as a function of temperature on the purely metallic surface. This concept is also implied by the QMS data in Fig.1, which show no strong hysteresis in the high temperature region >700 K, i.e. the strong hysteresis effects at temperatures below 700 K are clearly related to the formation and decay of the dissolved carbon phase. From TPD studies of oxygen desorption from Pd(111) [45,46] it is known that chemisorbed oxygen starts to desorb at around 650 K and reaches a rate maximum at ~720 K. This opens an additional reaction channel to decrease the (unmeasurably low) steady oxygen surface coverage at around 800 K and may explain the gradual selectivity shift toward CO above 750 K.

4.2. Cooling cycle

Down to ~720 K only little hysteresis is observed, and the arguments presented already for region C) of the heating cycle above ~720 K hold. In contrast to the heating cycle, below 720 K a general trend towards more CO_2 (Fig. 8, strong CO_2 maximum at 600 K in Fig.1) and less CO is clearly observed. This trend is related to the delayed formation of the Pd_xC_y phase at T~550 K during cooling (Fig.8). An increasing lifetime of CO(ads) from 720 K to <600 K on the predominantly metallic surface may explain the strong increase of the CO_2 formation rate and selectivity at least down to ~550 K. During heating in the same temperature region mainly the dissolved carbon state of the catalyst was present, leading to preferential CO formation. The Pd_xC_y intensity reaches its maximum during cooling at <500 K, but at this temperature the reaction rate already approaches zero, as can be deduced from Fig.1. Therefore it is likely that the Pd_xC_y phase is formed at a too low temperature to contribute substantially to the reaction rate and the selectivity pattern of the metallic surface is predominant.

5. Conclusions

Ethene oxidation is catalyzed by both the metallic and the dissolved carbon (electronically altered) phase, which preferentially catalyzes CO formation. The observed selectivity hysteresis is a consequence of the delayed buildup of this phase during cooling. Two main reasons may be discussed for the high selectivity on Pd_xC_y toward CO: (1) since reactive C atoms are ubiquitous in the dissolved carbon state of the catalyst the steady coverage of adsorbed oxygen may be rather low, and (2) a reduced lifetime of CO on the electronically altered surface may specifically favour the CO desorption channel.

Since CO is already a "partial" oxidation product, the importance of the carbon-loaded Pd catalyst for partial oxidation processes is supported (although no molecular reaction products such as acetic acid or acetaldehyde could be quantified in this study for experimental reasons). In this respect the particular importance of an oxygen-depleted, but carbon-enriched catalyst, which remains in a highly reduced state, despite of the relatively high partial pressure of oxygen, may be rather spotted in the suppression of ethene dissociative adsorption.

Acknowledgement

This work was supported by the European Community - Research Infrastructure Action under the FP6 "Structuring the European Research Area" Programme (through the Integrated Infrastructure Initiative" Integrating Activity on Synchrotron and Free Electron Laser Science - Contract R II 3-CT-2004-506008). The work was also supported by Enterprise Ireland through International Collaboration Programme (IC/2004/099). DZ received a research scholarship from the Foundation of the University of Limerick. HG acknowledges a grant from the Max Planck Society. We gratefully acknowledge BESSY staff for the support during the beamtime.

References

[1] A.K. Datye, J. Bravo, T.R. Nelson, P. Atanasova, M. Lyubovsky, L. Pfefferle, Applied Catalysis, A: General 198 **(2000)** 179-196.
[2] R.J. Farrauto, M.C. Hobson, T. Kennelly, E.M. Waterman, Applied Catalysis, A: General 81 **(1992)** 227-37.
[3] P. Salomonsson, S. Johansson, B. Kasemo, Catal. Lett. 33 **(1995)** 1.
[4] G.B. Hoflund, H.A.E. Hagelin, J.F. Weaver, G.N. Salaita, Appl. Surf. Sci. 205 **(2003)** 102-112.
[5] W. Unterberger, H. Gabasch, K. Hayek, B. Kloetzer, Catal. Lett. 104 **(2005)** 1-8.
[6] H.R. Gerberich, N.W. Cant, W.K. Hall, J. Catal. 16 **(1970)** 204-19.
[7] J. Xie, Q. Zhang, K.T. Chuang, Catal. Lett. 93 **(2004)** 181-184.
[8] B. Samanos, P. Boutry, R. Montarnal, J. Catal. 23 **(1971)** 19-30.
[9] Y.F. Han, D. Kumar, D.W. Goodman, J. Catal. 230 **(2005)** 353-358.
[10] Y.F. Han, D. Kumar, C. Sivadinarayana, A. Clearfield, D.W. Goodman, Catal. Lett. 94 **(2004)** 131-134.
[11] [11] D. Stacchiola, F. Calaza, L. Burkholder, W.T. Tysoe, J. Am. Chem. Soc. 126 **(2004)** 15384-15385.
[12] [12] M. Bowker, C. Morgan, Catal. Lett. 98 **(2004)** 67.
[13] [13] M. Morkel, G. Rupprechter, H.-J. Freund, Surf. Sci. Lett. 588 **(2005)** L209.
[14] S.B. Ziemecki, G.A. Jones, D.G. Swartzfager, R.L. Harlow, J. Faber Jr., J. Am. Chem. Soc. 107 **(1985)** 4547.
[15] R.H. Siller, W.A. Oates, R.B. McLellan, Journal of Less-Common Metals 16 **(1968)** 71.
[16] Z. Paál, U. Wild, R. Schlögl, Phys.Chem. Chem. Phys. 3 **(2001)** 4644.
[17] M. Todorova, W.X. Li, M.V. Ganduglia-Pirovano, C. Stampfl, K. Reuter, M. Scheffler, Phys. Rev. Lett. 89 **(2002)** 096103/1-096103/4.
[18] I.V. Yudanov, K.M. Neyman, N. Roesch, Physical Chemistry Chemical Physics 6 **(2004)** 116-123.
[19] H. Gabasch, K. Hayek, B. Kloetzer, A. Knop-Gericke, R. Schloegl, Journal of Physical Chemistry B 110 **(2006)** 4947-4952.
[20] M.K. Rose, A. Borg, T. Mitsui, D.F. Ogletree, M. Salmeron, J. Chem. Phys. 115 **(2001)** 10927-10934.

[21] L. Gracia, M. Calatayud, J. Andres, C. Minot, M. Salmeron, Physical Review B: Condensed Matter and Materials Physics 71 **(2005)** 033407/1-033407/4.
[22] R.W. Joiner, M.W. Roberts, Chem. Phys. Lett. 60 **(1979)** 459.
[23] V.I. Bukhtiyarov, V.V. Kaichev, I.P. Prosvirin, Topics in Catalysis 32 **(2005)** 3-15.
[24] R. Wuerz, M. Rusu, T. Schedel-Niedrig, M.C. Lux-Steiner, H. Bluhm, M. Haevecker, E. Kleimenov, A. Knop-Gericke, R. Schloegl, Surf. Sci. 580 **(2005)** 80-94.
[25] R. Schloegl, D. Teschner, A. Knop-Gericke, M. Haevecker, E. Kleimenov, D. Su, Abstracts of Papers, 228th ACS National Meeting, Philadelphia, PA, United States, August 22-26, 2004 **(2004)** COLL-194.
[26] H. Bluhm, M. Haevecker, A. Knop-Gericke, E. Kleimenov, R. Schloegl, D. Teschner, V.I. Bukhtiyarov, D.F. Ogletree, M. Salmeron, Journal of Physical Chemistry B 108 **(2004)** 14340-14347.
[27] D. Teschner, A. Pestryakov, E. Kleimenov, M. Haevecker, H. Bluhm, H. Sauer, A. Knop-Gericke, R. Schloegl, J. Catal. 230 **(2005)** 186-194.
[28] A. Bayer, K. Flechtner, R. Denecke, H.-P. Steinrueck, K.M. Neyman, N. Roesch, Surf. Sci. 600 **(2005)** 78-94.
[29] J.N. Andersen, D. Hennig, E. Lundgren, M. Methfessel, R. Nyholm, M. Scheffler, Phys. Rev. B: Condens. Matter 50 **(1994)** 17525-33.
[30] F.P. Leisenberger, G. Koller, M. Sock, S. Surnev, M.G. Ramsey, F.P. Netzer, B. Klotzer, K. Hayek, Surf. Sci. 445 **(2000)** 380-393.
[31] M. Bowker, C. Morgan, N. Perkins, R. Holroyd, E. Fourre, F. Grillo, A. MacDowall, Journal of Physical Chemistry B 109 **(2005)** 2377-2386.
[32] M. Sock, A. Eichler, S. Surnev, J.N. Andersen, B. Klotzer, K. Hayek, M.G. Ramsey, F.P. Netzer, Surf. Sci. 545 **(2003)** 122-136.
[33] M. Nishijima, J. Yoshinobu, T. Sekitani, M. Onchi, J. Chem. Phys. 90 **(1989)** 5114-27.
[34] S. Surnev, M. Sock, M.G. Ramsey, F.P. Netzer, M. Wiklund, M. Borg, J.N. Andersen, Surf. Sci. 470 **(2000)** 171-185.
[35] R.D. Haley, M.S. Tikhov, R.M. Lambert, Catal. Lett. 76 **(2001)** 125-130.
[36] D. Zemlyanov, B. Aszalos-Kiss, E. Kleimenov, D. Teschner, S. Zafeiratos, M. Haevecker, A. Knop-Gericke, R. Schloegl, H. Gabasch, W. Unterberger, K. Hayek, B. Kloetzer, Surf. Sci. 600 **(2006)** 983-994.
[37] M. Rocca, F. Moresco, Prog. Surf. Sci. 53 **(1997)** 331-340.
[38] M. Rocca, S. Lizzit, B. Brena, G. Cautero, G. Comelli, G. Paolucci, J. Phys.: Condens. Matter 7 **(1995)** L611-L618.
[39] F.P. Netzer, M.M. El Gomati, Surf. Sci. 124 **(1983)** 26-38.
[40] S. Tanuma, C.J. Powell, D.R. Penn, Surf. Interface Anal. 17 **(1991)** 911-26.
[41] Z. Ferhat-Hamida, J. Barbier, Jr., S. Labruquere, D. Duprez, Applied Catalysis, B: Environmental 29 **(2001)** 195-205.
[42] B. Kloetzer, W. Unterberger, K. Hayek, Surf. Sci. 532 **(2003)** 142.
[43] X. Guo, J.T. Yates, Jr., J. Chem. Phys. 90 **(1989)** 6761-6.
[44] D.L.S. Nieskens, M.M.M. Jansen, A.P. van Bavel, D. Curulla-Ferre, J.W. Niemantsverdriet, Phys. Chem. Chem. Phys. 8 **(2006)** 624-632.
[45] B. Klotzer, K. Hayek, C. Konvicka, E. Lundgren, P. Varga, Surf. Sci. 482-485 **(2001)** 237-242.
[46] H. Gabasch, W. Unterberger, K. Hayek, B. Kloetzer, G. Kresse, C. Klein, M. Schmid, P. Varga, Surf. Sci. 600 **(2005)** 205-218.